

CALIBRATION OF AN SEM, USING A NANO POSITIONING TILTING TABLE AND A MICROSCOPIC CALIBRATION PYRAMID

Olaf Sinram^a, Martin Ritter^b, S. Kleindiek^c, A. Schertel^d, H. Hohenberg^b and J. Albertz^a

^aTU Berlin, Photogrammetry and Cartography, D-10623 Berlin, Germany, sinram@fpk.tu-berlin.de

^bHPI Hamburg, Electron Microscopy Group, D-20251 Hamburg, Germany, ritter@hpi.uni-hamburg.de

^cKleindiek Nanotechnik, D-72770 Reutlingen, Germany

^dFEI GmbH, D-85622 Feldkirchen-Munich, Germany

Commission V, WG 2

KEY WORDS: Adjustment, Calibration, Photogrammetry, Orientation, Bundle, Close Range

ABSTRACT:

In this paper we present the calibration of a scanning electron microscope, using a high precision tilting sample stage and a new microscopic calibration pyramid. Difficulties when using extremely high magnifications will be stated and means of solutions are presented and evaluated. Since the scanning electron microscope cannot be moved around the object, the object has to be tilted instead. By this movement, the object can be seen in several virtual points of view, which is a necessity for any three dimensional reconstruction. As for generating the virtual views, the first difficulty encountered is to position the sample into the eucentric axis. Only when positioned in the rotation axis, the sample remains within the field of view, instead of being moved outside. Therefore, a special tilting table was required, which provided maximum precision and accuracy. Furthermore, an object had to be found, which met the requirements of a calibration object. Here, a new microscopic cascade pyramid was developed, supplied with 38 spatially distributed control points. Finally, for each tilting series, all desired images were oriented using a bundle block adjustment following the rules of parallel projection. In this paper, the mathematics of parallel projection will be an important chapter, pointing out the differences to central projection. As a result, the accuracy of the tilting table and the imaging properties of the microscope are presented. These properties are used as the basic essential parameters for further evaluation of microscopic images.

KURZFASSUNG:

In dieser Arbeit stellen wir die Kalibrierung eines Rasterelektronenmikroskops vor, bei der wir einen kippenauen Probenstisch und eine neuartige mikroskopische Stufenpyramide als Kalibrierkörper verwenden. Die Probleme, die sich stellen, wenn man bei extrem hohen Vergrößerungen arbeitet, sollen aufgezählt und Lösungswege vorgestellt und beurteilt werden. Da das Mikroskop nicht um das zu untersuchende Objekt herum bewegt werden kann, muss statt dessen das Objekt gekippt werden um virtuelle Kamerastandpunkte, die für jede räumliche Auswertung eine Grundvoraussetzung sind, zu erhalten. Bei der Generierung der virtuellen Aufnahmeanordnung durch die Kippung, wird die Schwierigkeit auftreten, die Probe in die euzentrische Achse zu bewegen. Nur direkt auf der Rotationsachse liegend, verbleibt die Probe bei der Drehung im extrem kleinen Sichtfeld, anstatt dieses zu verlassen. Um diese Anforderungen zu erfüllen, wurde ein hochpräziser und zuverlässig genauer Kipptisch benötigt. Zudem musste ein Objekt gefunden werden, welches den Ansprüchen für ein Kalibrierobjekt genügt. Es wurde daher eine Stufenpyramide entwickelt, die mit 38 räumlich verteilten Passpunkten ausgestattet ist. Schließlich wurden alle ausgewählten Bilder einer Kippserie durch eine Bündelblockausgleichung orientiert, die in unserem Falle den Gesetzen der Parallelprojektion folgt. Die Mathematik der Parallelprojektion stellt in dieser Arbeit ein wichtiges Kapitel dar, in welchem des weiteren die Unterschiede zur Zentralprojektion erklärt werden sollen. Als Ergebnis stellen wir die Genauigkeit des Kipptisches und die Abbildungseigenschaften des Mikroskops vor, welche die Ausgangsparameter für jede folgende räumliche Auswertung bilden.

1. INTRODUCTION

The surface reconstruction of biological objects is the motivation for exploiting the possibilities modern microscopic techniques are offering. At the Technical University of Berlin in cooperation with the Heinrich-Pette-Institut in Hamburg a research project under the title "photogrammetric reconstruction of biological surfaces on the basis of SEM Data" is currently sponsored by the Deutsche Forschungsgemeinschaft.

The reconstruction of real world objects can be achieved in various ways. Photogrammetry offers means for non-destructive reconstruction since the object, being depicted is not touched. The derivation of spatial coordinates is done indirectly through the images. This becomes especially interesting, if the sample of interest is very sensitive to tactile treatment, or may even suffer geometric distortions.

Cellular biological samples are very small. Only few options remain to capture the sample properties. Among others, optical microscopy, electron microscopy and AFM are to be mentioned. For a brief overview see (Hemmler, 2001). In this project we will explore the properties of SEM images for further evaluation. The SEM has always been an interesting approach for photogrammetry, since it provides a large depth of focus and images can be captured over a wide range of magnification, very much in contrast to optical microscopes. Also, the good signal to noise ratio makes them a first choice for evaluation. Since the data are generated digitally (Koenig et. al., 1987) it is a good basis for automation. A brief overview about how SEM images are generated will be given in the next chapter (Maune, 1976).

There are some preconditions to spatial object reconstruction. The sensor has to be mathematically modelled, hence the imaging properties have to be known. Additionally, two or more images, of which the orientation parameters have to be supplied are required to derive three dimensional coordinates. These requirements raise two difficulties: First, ways to achieve different point of views have to be found, since it is impossible to move the microscope around the sample. Second, an object that serves as a calibration standard has to be used. Also for implementation, the calibration standard should approximately match the object size of later samples. Chapter 2.2 will introduce the nano positioning tilting table as a solution to the first obstacle. The recently developed microscopic calibration standard will be shown in chapter 2.3.

When using magnifications of 1000x and higher in the SEM, parallel projection can be assumed (Hemmler, 2001). Therefore, not only the interior and exterior orientation parameters will change, but also the mathematic approach to compute them. Details will be explained in chapter 3.

2. HARDWARE COMPONENTS

2.1 The Scanning Electron Microscope

An electron beam generated on top of the microscope is accelerated with up to several thousand volts. Using a system of electronic lenses and coils, the beam is focused in the microscope column and scanned over a chosen area of the sample surface. The important signal component consists of so-called secondary electrons (SE), which are generated within the sample surface when hit by the electron beam. As the exit depth of SE is rather small, they carry high-resolution information. A positively charged detector collects the secondary electrons emitted at any scan position. According to the SE intensity at a given scan position, an analogous signal is generated and sent to a cathode ray tube, the screen. Mostly SE are responsible for the topographic contrast in SEM images as used here. This results mainly from the dependence of the SE yield on the tilt angle of the local surface normal relative to the incident beam.

The shorter wavelength of electrons compared to visual light allows a resolution in the nanometer range. In combination with the introduced advantages, like depth of focus and good signal-to-noise ratio, SEM images are very interesting to photogrammetric applications. The law of projection to be applied is depending on the magnification. While the scanning electron beam can be considered as central projective, it should be interpreted as parallel projective above a magnification of 1000x and more. The consequences to the mathematical models will be explained in chapters 2.3 and chapter 3.

2.2 The Nano Positioning Tilting Table

We already mentioned the necessity to simulate different points of view in order to derive 3D coordinates. As the specimen is positioned inside the vacuum chamber of the microscope, it is in a way a part of the microscope itself. In this special case, we are not able to move the camera around the object. Instead, we have to tilt the sample along a rotation axis in order to allow views from different positions. Due to the fact that the field of view in an SEM is extremely small, any translation of the sample is unwanted. Rotating the sample, respectively the sample stage, may result easily in a translation motion, if the area of interest is not positioned within the rotation axis, the so-called eucentric axis, as shown in fig.1. Therefore, a way to very accurately move the sample into the eucentric axis had to be found.

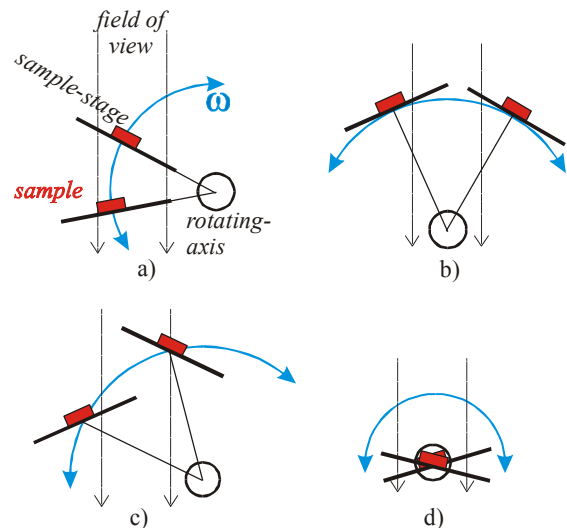


Figure 1. The effects of rotating a sample variously positioned with regard to the rotation axis: Situation a) and c) show a shifting along the z-axis, resulting in problems to the focus. The sample is displaced along the x-axis from the rotation axis in situation b) and c), causing the area of interest to exit the field of view. In situation d) finally, only the tilting of the sample will be observed.

A nano positioning tilting table has recently been developed to reliably move the sample into the desired position as depicted in Figure 1.d), even at magnifications higher than 50000x. The dimensions of the microscopes vacuum chamber limit the design of the tilting table. Figure 2 shows an actual photograph of the table. To give an idea of the table's dimension, a 10 Euro-Cent coin has been placed next to the table, in the lower right corner of the image.

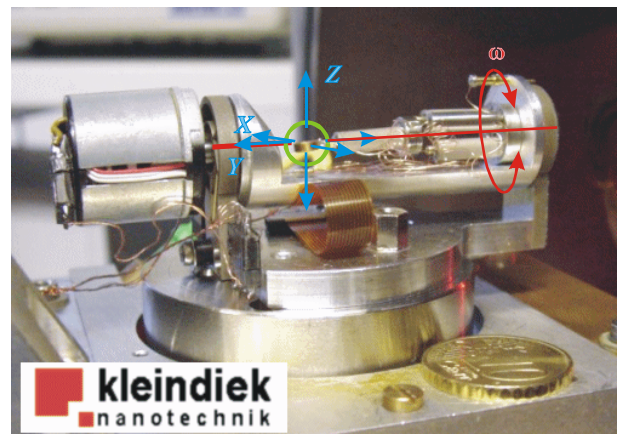


Figure 2. Photograph of the positioning tilting table, showing the rotation axis (red), the translation axes (blue) and enhancing the actual sample stage (green).

With this nano-positioning tool, the operator of the microscope is able to move the area of interest interactively into the desired position. However, despite the accuracy and reliability of the positioning table it remains an iterative process, challenging the operators patience.

2.3 The Microscopic Calibration Pyramid

For the calibration of the sensor and the verification of the table a reference object is necessary. The object has to be small enough to correspond to the approximate magnification of subsequent evaluation projects. Additionally, definite control points with known spatial coordinates have to be identified. The first obvious choice was a regular 2D grid. But we encountered problems with mathematical ambiguities due to the parallel projection model. Figure 3 illustrates these ambiguities, in contrast to central projection.

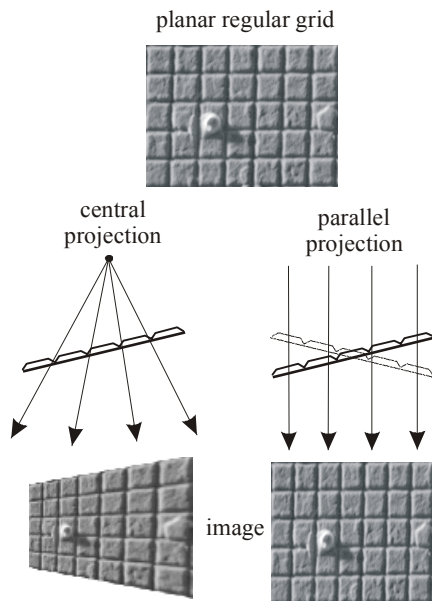


Figure 3. Ambiguities when projecting 2D objects with parallel projection. While the central perspective image is non-ambiguous (left), the parallel projection gives the same result, when the sample is tilted in either direction, or even if the image is scaled in one direction.

Therefore, a two dimensional object was not found suitable, although such specimen are easy to acquire and offered in a large variety from different providers. Consequently an object offering spatially distributed control points (nanomarkers) was required. A cascade pyramid with sloping edges was developed with 21 nanomarkers on the bottom level, 12 markers on the middle and 5 markers on the top level, serving as well distinguishable control points. The distribution on the lower level is non-symmetrical to be always informed of the pyramid's orientation. Figure 4 shows that the imaging ambiguities due to parallel projection are resolved with the use of such a pyramidal shaped calibration object. From the images we are able to derive the non-ambiguous tilting angles and eventually significant affine distortion parameters.

Figure 4 also shows that due to the objects sloping edges, nanomarker points will only be invisible, when extremely tilted. The slopes being vertical, nanomarker points would easily be covered by higher pyramidal stages at low tilting angles.

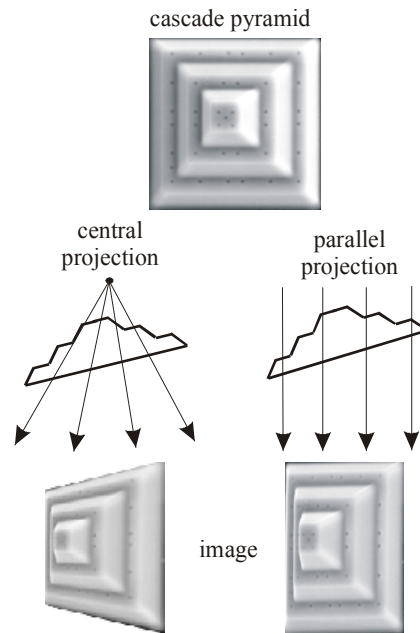


Figure 4. Central and parallel projection deliver a non-ambiguous result with three dimensional objects.

Another advantage of the sloping edges is the ability to measure the spatial coordinates of the nanomarkers with an atomic force microscope (AFM). The sensor of an AFM consists of a tip with a radius of only a few nanometers. Due to the tip shape, it is difficult to measure vertical structures. With the calibration structure developed for this project, the AFM can access all the nanomarkers. Figure 5 finally shows an SEM image of the pyramid.

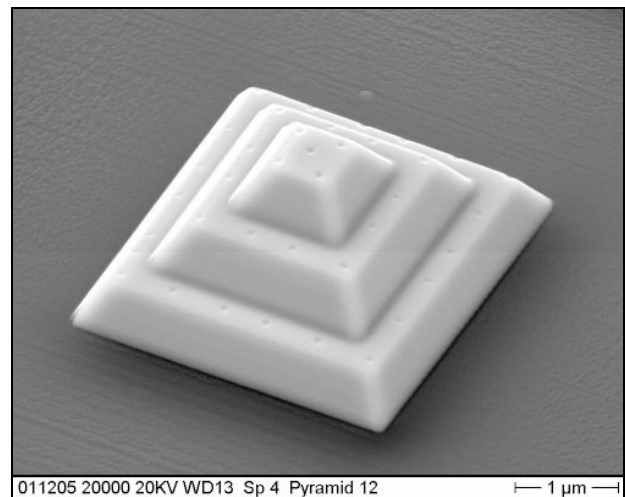


Figure 5. SEM image of the calibration pyramid

Such a pyramid approximately measures $6\mu\text{m}$ in width and length and $2\mu\text{m}$ in height. To give an idea about the real dimensions: if the pyramid had the size of a One Euro coin, this coin would correspond the diameter of a soccer field and be 9 meters in height. This might help understanding the difficulties of moving and keeping the specimen in the eucentric axis.

3. PHOTOGRAMMETRIC RESTITUTION

3.1 Parallel Projection

As we have mentioned, we will now consider parallel projection to be the normal case in microscopic imagery. Several works have shown, that errors due to the projection model are smaller than errors in image point measurement at magnifications of approximately 1000x and more.

The mathematics have to be adapted to the different model. This will include the bundle block adjustment and any subsequent section in space.

First we will examine how the interior and exterior parameters of the sensor and the images change.

Since the ray of sights are parallel they will not merge in one central point, hence there is no more projection centre. The missing projection centre has effects on both, the sensor and the image. On the sensor we can no longer construct a perpendicular on the image plane, known as the principal point. Also there cannot be a calibrated focal length anymore, i.e. the distance from the principal point to the projection centre. Instead the image is described by a global scaling factor. So the number of unknowns per sensor has dropped from three to one. However, additional parameters like radial and tangential lens distortion, or affine transformation parameters may still be applied (Elghazali, 1984). The global scaling factor, which substitutes the calibrated focal length is also the mathematical explanation for the ambiguities described in figure 3, in contrast to central projection, where each point has an individual scaling factor, depending on its spatial distance from the projection centre. Since in case of parallel projection each image point has the same global scaling factor, the object points distance has no influence on the images geometry anymore. Hence, the tilting direction of planar shapes is not distinguishable.

Due to the missing of a projection centre, we cannot clearly define the position of the image plane in object space. While the parameters of the rotation remain unchanged, it is sufficient to give a two dimensional offset along the x-y-plane to represent the imaging situation exactly. The z-component may be dropped since any image along the line of sight will give the same result. So the number of unknowns per image is now five instead of six. In figure 6 the geometry of parallel projection with its consequences is illustrated.

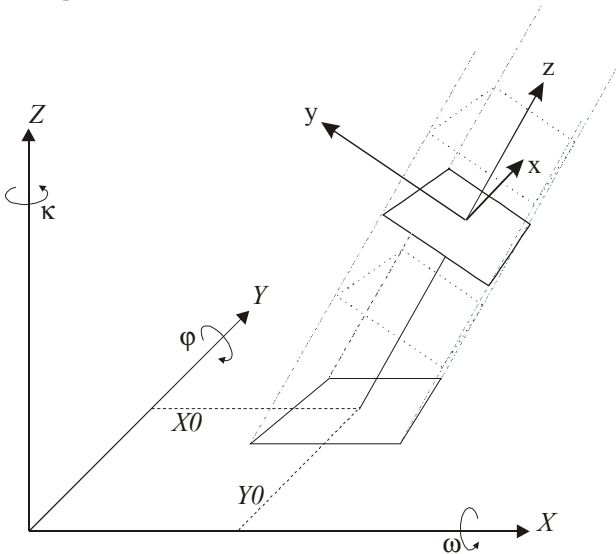


Figure 6. Parallelprojective geometry

3.2 Parallel Block Adjustment

After making clear why and how the geometry changes, we would like to describe the differences mathematically.

Previous works often used the samples tilting angle as the only parameter for the three dimensional object reconstruction. The forward section was simplified to this assumption and the use of two images was enough (Hemmler, 1996; Burkhardt 1981). In this work we want to extend the mathematical model to full flexibility for several reasons. First, the parallel block adjustment provides us with highly accurate results in image orientation and sensor properties. This way small errors in the sample tilting process are modelled by the rotation angles as well. These results will be applicable to any arbitrary image setup. So this flexibility takes into consideration any future hardware development, which may allow specimen movement along more than one axis.

Additionally, any accurate subsequent section in space requires full knowledge of the image orientations. The formulas which are introduced later, will show an approach to derive accurate object points from an arbitrary number of images. So not only the accuracy is enhanced by taking advantage of observations in several images, but we are also able to check for blunders, as will be explained later in this chapter.

As mentioned above we now have to consider 5 unknowns for each image and only one unknown for each sensor.

In the following, the image coordinates will be given in pixels, related to the digital images centre. Hence the scale factor has the unit $pixel/\mu m$, or $pixel/nm$ respectively.

The collinearity equation for parallel perspective will be as follows:

$$\begin{pmatrix} \textcircled{R}x \\ \textcircled{C}y \\ \textcircled{C}y \\ \textcircled{m} \end{pmatrix} = m \cdot R \cdot \begin{pmatrix} \textcircled{R}X - X_0 \\ \textcircled{C}Y - Y_0 \\ \textcircled{C}Y - Y_0 \\ \textcircled{m} Z \end{pmatrix} \quad (1)$$

$$x = m[R_{11}(X - X_0) + R_{21}(Y - Y_0) + R_{31}Z]$$

$$y = m[R_{12}(X - X_0) + R_{22}(Y - Y_0) + R_{32}Z]$$

where m = scaling factor

x, y = image coordinates

X, Y, Z = object coordinates

X_0, Y_0 = projection centre (see Fig. 6)

R = Rotation matrix

The following model will be used as a Rotation matrix:

$$R_{\varphi\omega\kappa} = \begin{pmatrix} \textcircled{C}\cos \varphi & 0 & \textcircled{C}\sin \varphi \\ \textcircled{C}0 & 1 & 0 \\ \textcircled{m}\sin \varphi & 0 & \textcircled{C}\cos \varphi \end{pmatrix} \cdot \begin{pmatrix} \textcircled{C}0 & 0 & 0 \\ \textcircled{C}\cos \omega & -\textcircled{C}\sin \omega \\ \textcircled{m}\sin \omega & \textcircled{C}\cos \omega \end{pmatrix} \cdot \begin{pmatrix} \textcircled{C}\cos \kappa & -\textcircled{C}\sin \kappa & 0 \\ \textcircled{C}\sin \kappa & \textcircled{C}\cos \kappa & 0 \\ \textcircled{m}0 & 0 & 1 \end{pmatrix} \quad (2)$$

When entering the parallel block adjustment, with observed image points x, y , given control point coordinates X, Y and the unknowns $\varphi, \omega, \kappa, X_0, Y_0$ and m , we have to apply the following observation equations:

$$\begin{pmatrix} \textcircled{R} \\ \textcircled{C} \\ \textcircled{C} \\ \textcircled{TM} \end{pmatrix} \begin{pmatrix} x \\ y \\ 0 \end{pmatrix} + \begin{pmatrix} \textcircled{R}'_x \\ \textcircled{C}'_y \\ \textcircled{TM}'_0 \end{pmatrix} = m \cdot R \cdot \begin{pmatrix} \textcircled{R} \\ \textcircled{C} \\ \textcircled{C} \\ \textcircled{TM} \end{pmatrix} \begin{pmatrix} X - X_0 \\ Y - Y_0 \\ Z \end{pmatrix} \quad (3)$$

The differentials for the error equation coefficients are given as follows for images, sensors and new points (∂y accordingly):

$$\begin{pmatrix} \textcircled{R} \\ \textcircled{C} \\ \textcircled{C} \\ \textcircled{TM} \end{pmatrix} \frac{\partial x}{\partial X_0} = -m \cdot R_{11} \quad (4a)$$

$$\begin{pmatrix} \textcircled{R} \\ \textcircled{C} \\ \textcircled{C} \\ \textcircled{TM} \end{pmatrix} \frac{\partial x}{\partial Y_0} = -m \cdot R_{21}$$

$$\begin{pmatrix} \textcircled{R} \\ \textcircled{C} \\ \textcircled{C} \\ \textcircled{TM} \end{pmatrix} \frac{\partial x}{\partial \varphi} = m \cdot \left(\frac{\partial R_{11}}{\partial \varphi} \cdot (X - X_0) + \frac{\partial R_{21}}{\partial \varphi} \cdot (Y - Y_0) + \frac{\partial R_{31}}{\partial \varphi} \cdot Z \right)$$

$$\begin{pmatrix} \textcircled{R} \\ \textcircled{C} \\ \textcircled{C} \\ \textcircled{TM} \end{pmatrix} \frac{\partial x}{\partial \omega} = m \cdot \left(\frac{\partial R_{11}}{\partial \omega} \cdot (X - X_0) + \frac{\partial R_{21}}{\partial \omega} \cdot (Y - Y_0) + \frac{\partial R_{31}}{\partial \omega} \cdot Z \right)$$

$$\begin{pmatrix} \textcircled{R} \\ \textcircled{C} \\ \textcircled{C} \\ \textcircled{TM} \end{pmatrix} \frac{\partial x}{\partial \kappa} = m \cdot \left(\frac{\partial R_{11}}{\partial \kappa} \cdot (X - X_0) + \frac{\partial R_{21}}{\partial \kappa} \cdot (Y - Y_0) + \frac{\partial R_{31}}{\partial \kappa} \cdot Z \right)$$

$$\begin{pmatrix} \textcircled{R} \\ \textcircled{C} \\ \textcircled{C} \\ \textcircled{TM} \end{pmatrix} \frac{\partial x}{\partial m} = R_{11} \cdot (X - X_0) + R_{21} \cdot (Y - Y_0) + R_{31} \cdot Z \quad (4b)$$

$$\begin{pmatrix} \textcircled{R} \\ \textcircled{C} \\ \textcircled{C} \\ \textcircled{TM} \end{pmatrix} \frac{\partial x}{\partial X} = m \cdot R_{11} \quad (4c)$$

$$\begin{pmatrix} \textcircled{R} \\ \textcircled{C} \\ \textcircled{C} \\ \textcircled{TM} \end{pmatrix} \frac{\partial x}{\partial Y} = m \cdot R_{21}$$

$$\begin{pmatrix} \textcircled{R} \\ \textcircled{C} \\ \textcircled{C} \\ \textcircled{TM} \end{pmatrix} \frac{\partial x}{\partial Z} = m \cdot R_{31}$$

3.3 Parallel Section in Space

With the previously derived orientation parameters, we are now able to do object reconstruction with large amounts of points which were not included in the parallel block adjustment. A linear forward section for central projection is shown in (Kraus, 1997; Moré, 2000). We have transferred it to the parallel case, using the following equations:

$$X = (A^T A)^{-1} (A^T L), \quad (5)$$

with

$$L = \begin{pmatrix} \textcircled{R}x + m \cdot R_{11} \cdot X_0 + m \cdot R_{21} \cdot Y_0 \\ \textcircled{C}y + m \cdot R_{12} \cdot X_0 + m \cdot R_{22} \cdot Y_0 \\ \textcircled{C} \\ \textcircled{TM} \end{pmatrix} \begin{pmatrix} X_0 \\ Y_0 \\ \vdots \end{pmatrix}$$

and

$$A = \begin{pmatrix} \textcircled{R}m \cdot R_{11} & m \cdot R_{21} & m \cdot R_{31} \\ \textcircled{C}m \cdot R_{12} & m \cdot R_{22} & m \cdot R_{32} \\ \textcircled{C} & \vdots & \vdots \\ \textcircled{TM} & \vdots & \vdots \end{pmatrix}$$

The above is a very fast way of computing three dimensional coordinates from an arbitrary number of images, since this adjustment is linear. Therefore neither approximate values are required, nor will there be an iteration.

The computation of errors, however, is not reliable with this method. A closer look at the error matrix $Q_{xx} = (A^T A)^{-1}$ reveals, that the observations do not take part in this matrix, hence all image points seem to have the same error. Other ways have been and are being explored to reveal blunders in the observations. A rather simple approach is to use the correction matrix $v = AX - L$ for the detection of errors. A more sophisticated, yet time consuming approach, is the computation of the shortest distance of the new point to the line of sight of each image. Since all lines of sight should merge in one point, these distances ought to be rather small and equal to each other. Analysis of the distances can help detecting blunders and the originating image.

As mentioned above, this is currently a topic of research with a growing variety of setup situations and point measurements.

4. RESULTS

The suggested methods have been applied to several projects, involving the tilting sample stage and some calibration objects. As expected, the best results could be achieved with the latest cascade pyramid. As an example, a typical tilting series will be stated, using 13 images with up to 38 measured control points, each. All images shared one sensor, where the radial lens distortion and affine transformation were kept unknown as additional parameters. Thus, the whole adjustment system had 70 unknowns and 966 observations. Some results are shown in table 1.

sensor	magnification [pixel / nm]	magnification error [pixel / nm]
XL30 FEG	94.559	0.116

image number	X_0 [nm]	m_{x0} [nm]	φ [°]	m_φ [°]
	Y_0 [nm]	m_{y0} [nm]	ω [°]	m_ω [°]
			κ [°]	m_κ [°]
1	2.621	0.004	0.261	0.22
	1.941	0.004	351.038	0.21
			88.550	0.06
2	2.640	0.004	0.171	0.21
	1.882	0.004	345.935	0.19
			88.332	0.06
3	2.460	0.004	359.838	0.22
	2.017	0.004	356.701	0.22
			88.628	0.06
4	2.675	0.004	359.993	0.21
	1.794	0.004	341.131	0.18
			88.279	0.07
5	2.452	0.004	359.042	0.22
	2.033	0.004	1.728	0.22
			88.694	0.06

Table 1. The first 5 images of the tilting series.

The above table exemplarily shows the first five images of the tilting series, mentioned before. The tilting sample stage was set to: 0°, 355°, 5°, 350°, 10°, etc. Comparison with the adjusted results proves the high accuracy of the positioning table. Furthermore it provides high stability and convenient handling in use. The pyramid allows precise measurement, therefore supporting accurate results. Nevertheless, deviations may occur

and are subject to detailed investigation. The sensor, however, was set to a scale factor of $84.7 \text{ pixels}/\mu\text{m}$, yet the adjustment showed $94.6 \text{ pixels}/\mu\text{m}$. This deviation is yet to be investigated for consistency. Eventually the sensor has to be readjusted, since the sensor specifications serve as approximate values for the later adjustment. Finally, the whole system setup is illustrated in figure 7.

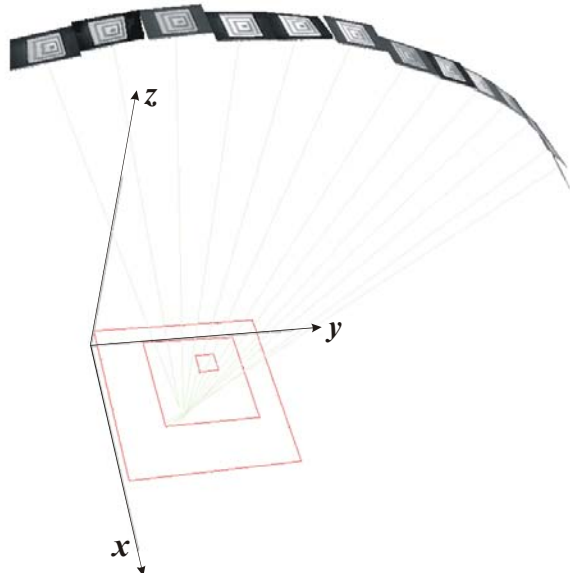


Figure 7. The system configuration visualized with VRML. The control points on each level of the pyramid have been connected with lines for means of clarification. For the same reason, the images have been moved away from the x,y-plane by the same distance (cp. figure 6).

5. CONCLUSIONS AND FUTURE WORK

The results we have achieved are very promising. The calibration pyramid is a very reliable and well recognizable object. In connection with the tilting stage it is possible to acquire series of images which give accurate information about both, the sensor properties and the tables consistency. The mathematical developments allow a very flexible system configuration. The current system is a very good basis for forthcoming evaluations. However, deviations and problems are known and are subject to investigation. Additionally, as mentioned before, the section in space is further investigated for stability and blunder detection. Future work will concentrate on the application of the introduced techniques to the evaluation of biological specimens. The calibration and orientation data will help optimising image correlation and will improve the accuracy of the result.

REFERENCES

- Burkhardt, R., 1981. Die stereoskopische Ausmessung elektronenmikroskopischer Bildpaare und ihre Genauigkeit. *Methodensammlung der Elektronenmikroskopie*, Abschnitt 4.2.2.
- Elghazali, M., 1984. System Calibration of Scanning Electron Microscopes. *International Archives of Photogrammetry and Remote Sensing*, Commission V, Vol. XXV, Part A5, pp. 258-266.
- Hemmler, M., Albertz, J., Schubert, M., Gleichmann, A., Köhler, J. M., 1996. Digital Microphotogrammetry with the Scanning Electron Microscope. *International Archives of Photogrammetry and Remote Sensing*, Commission V, Vol. XXXI, Part B5, pp. 225-230.
- Hemmler, M., 2001. *Photogrammetrische Auswertung elektronenmikroskopischer Bilddaten*. Ph.D. Thesis, Technical University of Berlin. http://edocs.tu-berlin.de/diss/2001/hemmler_matthias.pdf
- Koenig, G., Nickel, W., Storl, J., Meyer, D., Stange, J. 1987. *Digital Stereophotogrammetry for Processing SEM Data*. SCANNING Vol. 9, pp. 185-193.
- Kraus, K., 1997. *Photogrammetrie - Band 1. Grundlagen und Standardverfahren*. Dümmler-Verlag, 6. Auflage, Bonn.
- Maune, D. F., 1976. Photogrammetric Self-Calibration of Scanning Electron Microscopes. *Photogrammetric Engineering and Remote Sensing*, Vol. 42, No. 9, pp. 1161-1172.
- Moré, J., 2000. *Untersuchungen zur kombinierten Ausgleichung geodätischer und photogrammetrischer Beobachtungen*. Diploma Thesis, Technical University of Berlin, Photogrammetry and Cartography (not published)

ACKNOWLEDGEMENTS

The authors would like to thank the Deutsche Forschungsgemeinschaft, for supporting our researches. Furthermore, we want to thank Andreas Döring, Institute for experimental Physics, University of Ulm, for kindly providing AFM measurements on the calibration standards.